

Site-Dilution in quasi one-dimensional antiferromagnet $\text{Sr}_2(\text{Cu}_{1-x}\text{Pd}_x)\text{O}_3$: reduction of Néel Temperature and spatial distribution of ordered moment sizes

K. M. Kojima,* J. Yamanobe, H. Eisaki, and S. Uchida

Department of Physics, University of Tokyo, Hongo 7-3-1, Bunkyo, Tokyo 113-0033, Japan

Y. Fudamoto, I.M. Gat, M.I. Larkin, A. Savici, and Y.J. Uemura
Department of Physics, Columbia University, New York, NY 10027, USA

G.M. Luke

Department of Physics and Astronomy, McMaster University, Hamilton, Ontario, L8S 4M1, CANADA

(Dated:)

We investigate the Néel temperature of Sr_2CuO_3 as a function of the site dilution at the Cu ($S = 1/2$) sites with Pd ($S = 0$), utilizing the muon spin relaxation (μSR) technique. The Néel temperature, which is $T_N = 5.4\text{K}$ for the undoped system, becomes significantly reduced for less than one percent of doping Pd, giving a support for the previous proposal for the good one-dimensionality. The Pd concentration dependence of the Néel temperature is compared with a recent theoretical study (S. Eggert, I. Affleck and M.D.P. Horton, *Phys. Rev. Lett.* **89**, 47202 (2002)) of weakly coupled one-dimensional antiferromagnetic chains of $S = 1/2$ spins, and a quantitative agreement is found. The inhomogeneity of the ordered moment sizes is characterized by the μSR time spectra. We propose a model that the ordered moment size recovers away from the dopant $S = 0$ sites with a recovery length of $\xi \approx 150 - 200$ sites. The origin of the finite recovery length ξ for the gapless $S = 1/2$ antiferromagnetic chain is compared to the estimate based on the effective staggered magnetic field from the neighboring chains.

PACS numbers: PACS numbers: 76.75.+i, 75.25.+z, 75.10.Jm

I. INTRODUCTION

The discovery of high- T_c cuprates has prompted theoretical and experimental investigations of low-dimensional spin systems with spin quantum number $S = 1/2$. There were a series of neutron diffraction studies reported in the high- T_c cuprate $\text{La}_{2-x}\text{Sr}_x\text{CuO}_4$ [1, 2], in which the dynamical spin correlation was measured. It was found that the inverse correlation length $\xi^{-1}(x, T)$ may be divided into the two terms: the temperature independent term $\xi^{-1}(x, 0)$ which is purely determined by the doping concentration and the doping independent term $\xi^{-1}(0, T)$ which follows the universal temperature dependence. In samples with Néel ordering, the correlation length diverges $\xi^{-1} \rightarrow 0$ at T_N , exhibiting long-range magnetic order. Recently, effect of static site dilution was also investigated in $\text{La}_2(\text{Cu}_{1-x}(\text{Mg}, \text{Zn})_x)\text{O}_4$ [3]. The Néel temperature was found to disappear at the classical percolation threshold $p_c = 0.407$, but the site-dilution dependence of T_N does not follow the mean-field calculation. The reduction of T_N , spin-stiffness ρ_s and the equal-time correlation length $\xi(x, T)$ were compared with the microscopic quantum mechanical calculations of the $S = 1/2$ Heisenberg model on a square lattice [3].

The localized holes in the lightly doped $\text{La}_{2-x}\text{Sr}_x\text{CuO}_4$ and the impurities in the site dilution in $\text{La}_2(\text{Cu}_{1-x}(\text{Mg}, \text{Zn})_x)\text{O}_4$ break the translational

symmetry. The ordered moment size of these systems should not be homogeneous in space. However, the signature of the spatial inhomogeneity of the ordered moment sizes in cuprates is difficult to detect in the momentum space, because the doped sites are randomly distributed, the spin quantum number S is small and the dimensionality is low. Consequently, the length scale relevant to the moment size distribution in the impurity doped cuprates has not been resolved by the previous neutron diffraction measurements.

Site dilution in the quasi one-dimensional spin systems exhibits more important features of the quantum spin systems. One peculiar effect of site dilutions in one-dimensional spin systems is the creation of a Néel order out of the singlet ground state, as discovered in the impurity doped spin-Peierls material CuGeO_3 [4, 5] and the 2-leg spin ladder material SrCu_2O_3 [6]. These discoveries have promoted the idea that the Néel state appears as a competing phase to the original spin-gapped singlet state of either spin-Peierls or the spin-ladder. As a result of competition, there exists a length scale which determines the spatial variation of the ordered moment sizes [7, 8]. In doped spin Peierls compounds, the spin decay length in the Néel ordered state is determined by the ratio between the spin-gap magnitude Δ and the intra-chain antiferromagnetic coupling J , such as $\xi/a = J/\Delta$ [7]. This suggests that the spatial inhomogeneity of the ordered moment size is a feature of the spin-gap, and may not appear in the regular quasi one-dimensional antiferromagnets with Néel order, which are gapless ($\Delta = 0$) and the correlation length diverges.

*Electronic address: kojima@phys.s.u-tokyo.ac.jp

Recently, a series of measurements of Cu benzoate, a compound with $S = 1/2$ one-dimensional chains, have identified the existence of an energy gap induced by the external magnetic field [9, 10]. The origin of the energy gap has been interpreted as the effect of the staggered magnetic field induced on the Cu sites by the combination of the anisotropic g -tensor and the external field [11]. This observation points out that the $S = 1/2$ spin chain, which has a singlet ground state and gapless excitations if isolated, may acquire a spin-gap under a certain type of perturbation. In quasi one-dimensional antiferromagnets, the most common perturbation to an isolated chain is the existence of inter-chain interactions J' . In the mean-field approximation, the inter-chain interaction induces an effective staggered magnetic field $B \approx zJ'\langle s_z \rangle$, where $\langle s_z \rangle$ and z are the magnetic order parameter and the number of the nearest neighboring chains, respectively. The inter-chain interaction causes the Néel order [12] which is gapless because of the translational symmetry of the system. With the impurity doping to the $S = 1/2$ spin-chain, the translational symmetry is broken and the hidden features of the effective staggered fields from the inter-chain interaction may appear in the form of the recovery length ξ of the ordered moment size. However, this problem is still an open question.

The site dilution should have a destructive effect in the long-range coherence of the Néel order, especially in low dimensions. The true one-dimensional chain becomes fragments of finite sizes upon impurity doping, and the long-range order becomes impossible. However, with the existence of inter-chain interactions, the destruction of magnetic ordering with site dilution may be moderated; the true disappearance of the Néel order may occur only at the percolation threshold for the three-dimensional lattice structure of the inter-chain interactions. Recently, Eggert *et al.* presented a theoretical estimate for the Néel temperature [13] as a function of the site dilution in the $S = 1/2$ quasi one-dimensional antiferromagnet. The predicted T_N exhibits a simple reduction as a function of the average chain length L . Eventhough the ground state of an isolated $S = 1/2$ chain is a singlet, there was no enhancement of the Néel temperature upon impurity doping, in contrast with the gapped $S = 1/2$ systems, such as the spin-Peierls systems and the spin-ladders.

In order to experimentally investigate the theoretical predictions about T_N , and the uniformity of the ordered moment sizes in the depleted spin-chains, we have performed an investigation of Pd-doped Sr_2CuO_3 . The cuprate Sr_2CuO_3 has received an attention as a model material of the $S = 1/2$ quasi one-dimensional antiferromagnet; its low Néel temperature $T_N = 5.4\text{K}$ [14] and the large in-chain interaction $J \sim 2200\text{K}$ [15, 16, 17] suggests its good one-dimensionality. The ordered moment size $\approx 0.06\mu_B$ has been obtained by neutron scattering and μSR measurements [14]. This value is strongly reduced from the full moment size ($= 1\mu_B$) expected for the $S = 1/2$ spins. The suppressed moment size of Sr_2CuO_3 follows the prediction based on the ‘‘chain mean-field’’

theory [12], which employs the rigorous results of the isolated chains and includes the weak inter-chain interaction as the mean-field. As the non-magnetic impurity at the Cu site, Zn or Mg substitutions are the first choice, as has been already performed in the two-dimensional cuprates [3]. However in Sr_2CuO_3 , Zn or Mg ions does not go into the Cu site. We have employed Pd ion instead; Sr_2CuO_3 has an isostructural compound Sr_2PdO_3 , in which the Pd^{2+} ions are in the low-spin ($S = 0$) state [18]. This compound has enables us to investigate the non-magnetic impurity doping to the $S = 1/2$ antiferromagnetic spin-chain.

The structure of this paper is as follows. In section II, we present the magnetic susceptibility data and the result of muon spin relaxation (μSR) measurement of $\text{Sr}_2(\text{Cu}_{1-x}\text{Pd}_x)\text{O}_3$. The Néel temperature was estimated from the temperature dependence of the muon relaxation rate. In section III, we calculate the magnetic field distribution expected for the depleted spin-chains with Néel order. We assume a zero-moment at the impurity site and a recovery length ξ to describe the recovery of the ordered moment size into the bulk chain. The calculated field distribution is Fourier transformed to obtain the μSR spectrum, and employed in the analysis of the nominally pure as well as the doped samples. Conclusions are presented in Section IV.

II. EXPERIMENTAL RESULTS

We grew single crystals of $\text{Sr}_2(\text{Cu}_{1-x}\text{Pd}_x)\text{O}_3$, employing the traveling-solvent floating-zone technique, with CuO as the solvent. Stoichiometric ratio of SrCO_3 , CuO and PdO powders are prepared, mixed in a mortar for an hour and pre-fired in air at 900°C in an Al_2O_3 crucible. The powder sample is again mixed and fired in air at 950°C , before formed into a pressed rod using a rubber tube and a water static press. The polycrystalline rod is fired on a Pt plate at 1050°C . It is important to harden the rod by firing at the highest temperature possible for a stable growth of single crystal in the floating-zone furnace. We employed a gold-mirror bi-focus furnace made by NEC.

The magnetic susceptibility of $\text{Sr}_2(\text{Cu}_{1-x}\text{Pd}_x)\text{O}_3$ crystal is shown in Fig. 1a, with the magnetic field applied parallel to the longest crystallographic axis. An increase of the Curie-Weiss component was observed as the Pd concentration increases. We assume the conventional form for the magnetic susceptibility:

$$\chi(T) = \frac{C}{T + \Theta_W} + \chi_0 \quad (1)$$

where C is the Curie term, Θ_W is the Weiss temperature and χ_0 describes the temperature independent susceptibility as a sum of Van Vleck paramagnetism and core diamagnetism.

The parameters to describe susceptibility are shown in Table I. The Curie term is shown as the concentration of

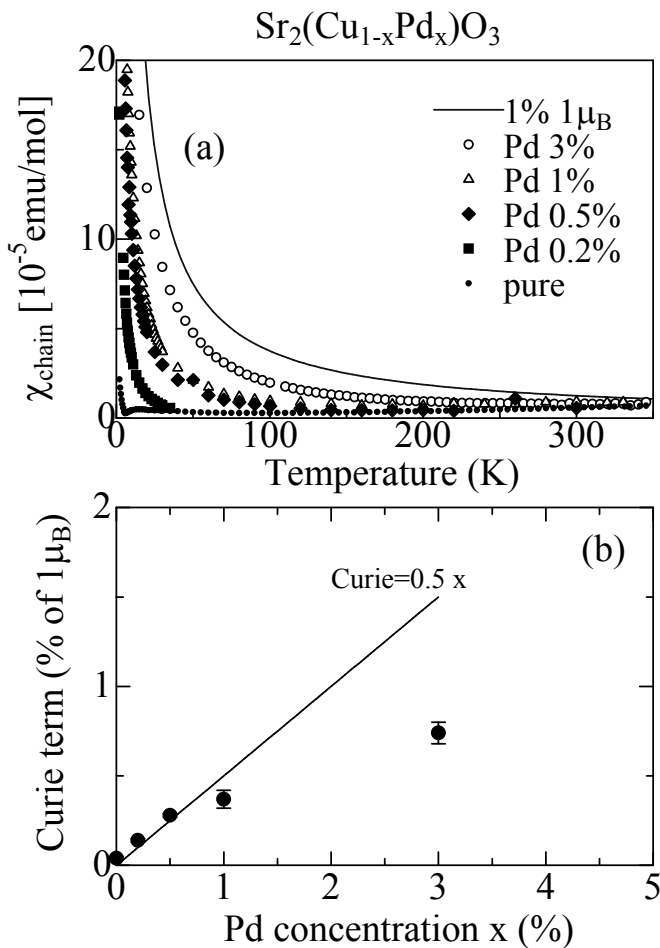


FIG. 1: (a) Magnetic susceptibility of single crystalline $\text{Sr}_2(\text{Cu}_{1-x}\text{Pd}_x)\text{O}_3$, with the magnetic field applied parallel to the longest crystallographic axis. (b) Pd concentration dependence of the Curie term. We note that the substitution with one Pd ion creates half an impurity moment assuming that the induced moment size is $1\mu_B$.

TABLE I: Parameters of susceptibility and μSR

Pd x (%)	Curie (%)	Θ_W (K)	χ_0 (emu/mol)	λ/ξ
0	0.04(1)	1.7	-1.8×10^{-5}	7.2 ^a
0.2	0.14(1)	0.8	-1.1×10^{-5}	(2.1) ^b
0.5	0.28(1)	0.03	-1.2×10^{-5}	(1.0)
1.0	0.37(5)	0.33	-1.3×10^{-5}	(0.78)
3.0	0.74(6)	2.1	-1.2×10^{-5}	(0.39)

^aobtained from an analysis of μSR spectrum (see Discussion).

^bnumbers in parenthesis are estimates from the Curie term.

the impurity moments which are assumed to be $1\mu_B$. The calculated concentrations of impurity moments are about *half* of the doped Pd concentration, as shown in Fig. 1b. This Pd concentration dependence of the Curie term may be explained as follows: One Pd ion creates one chain fragment. Assuming that the intra-chain interaction J is much larger than the interaction between the chain fragments, the total spin quantum number of the chain

fragment is well defined: it takes either $S = 0$ or $S = 1/2$ value, depending on the length of the fragment being an even or odd number of spin sites, respectively [13]. The observed Pd concentration dependence of the Curie term is consistent with the idea that it originates from the total spin of the created chain fragments. The Weiss temperature Θ_W exhibits a non-monotonic dependence on the Pd concentration. The origin of this dependence is unknown, however, its temperature scale is at most $\Theta_W \sim 2$ K, which is being significantly smaller than the intra-chain interaction $J \sim 2200$ K. This suggests that the interaction between the chain fragments are negligible compared to the intra-chain interaction, satisfying the condition assumed in the theory [13], which is compared with our measurement in the discussion section.

It is known that the Néel order of Sr_2CuO_3 is not detectable by magnetic susceptibility [17]. This is probably because of the very small ordered moment size $\approx 0.06\mu_B$. This feature of the material requires employing the muon spin relaxation (μSR) technique, which has the highest sensitivity among other experimental techniques to detect the magnetic order with small and/or dilute magnetic moments. We performed zero-field muon spin relaxation measurement on $\text{Sr}_2(\text{Cu}_{1-x}\text{Pd}_x)\text{O}_3$ crystals at M15 beam line of TRIUMF (Vancouver, Canada). Muons with 100% spin polarization were injected into the single crystalline sample with the initial polarization parallel to the longest crystallographic axis. This geometry is the same as the one employed in the previous measurement of nominally pure Sr_2CuO_3 [14]. The time evolution of muon spin polarization in zero-field is shown in Fig. 2a.

In undoped Sr_2CuO_3 , muon spin precession was observed as a consequence of Néel ordering [14]. This indicates that the ordered moment size is relatively homogeneous in space, and the local field at the muon sites is well defined. Upon Pd doping, the muon spin precession disappears and the time evolution of muon spin is dominated by the relaxation which has an approximately exponential behavior as a function of the time. Such exponential relaxation signal in zero-field comes from the $1/T_1$ relaxation caused by spin fluctuations, or alternatively from static fields of spatially distributed magnetic moments. The dynamic and static situations for the muon spin relaxation may be distinguished by the “decoupling” measurements under longitudinal fields applied parallel to the initial muon spin polarization [19]. The results are shown in Fig. 2b for the $x = 1.0\%$ specimen, together with the analysis using the static relaxation in Lorentzian field distribution [20]. It is clear that the relaxation is caused by the static field distribution, as is evident from the time-independent behavior in the long terms [20]. This leads to the conclusion that the muon spin relaxation is caused by a magnetic order.

We analyze the zero-field muon spin relaxation $P_\mu(t)$ in the doped samples utilizing the phenomenological function:

$$P_\mu(t) = \exp\left(-\frac{1}{2}(\Delta_{ndt})^2\right) \exp(-\lambda_{mag}t) \quad (2)$$

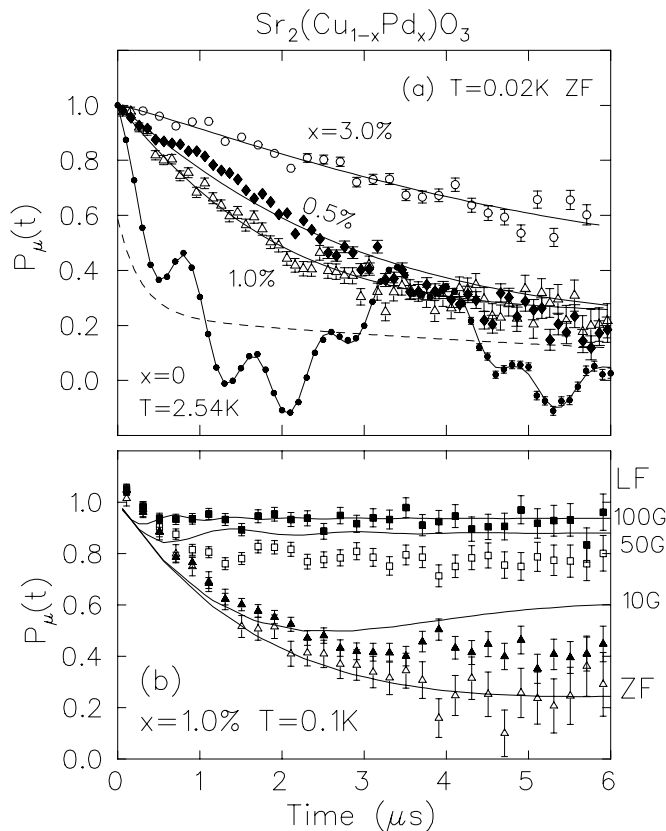


FIG. 2: (a) Zero-field muon spin relaxation in $\text{Sr}_2(\text{Cu}_{1-x}\text{Pd}_x)\text{O}_3$. The solid lines for the doped samples are the fits using eq. (2). On the spectrum of the samples with $x=0$, the solid line is a plot of eq.(1) in Ref.[14]. The dashed line is the sum of two exponential functions to describe the background relaxation. (b) Muon spin relaxation in longitudinal field ($H \parallel P_\mu(t)$) for the $x=1.0\%$ sample. The solid lines are the Lorentzian functions in the longitudinal fields used in the analysis.

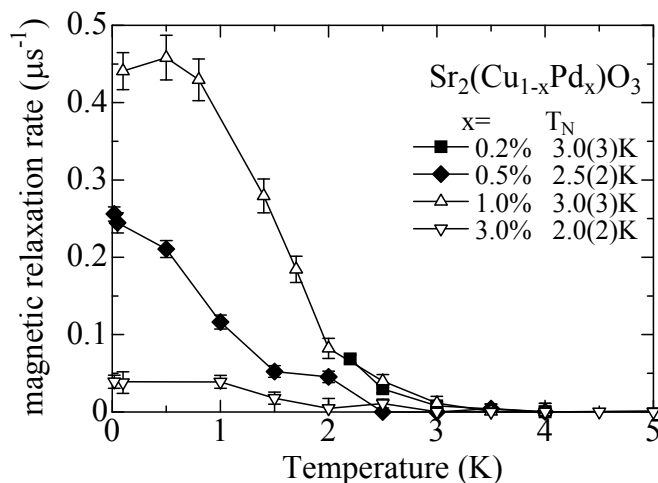


FIG. 3: Temperature dependence of the exponential relaxation rate for $\text{Sr}_2\text{Cu}_{1-x}\text{Pd}_x\text{O}_3$. The Néel temperatures are estimated from the temperature points where the relaxation rate start to rise.

as shown by the solid lines in Fig. 2a. In the analysis, the Gaussian relaxation was assumed to describe the static nuclear dipolar-fields, and was set to $\Delta_{nd} = 0.12\mu\text{s}^{-1}$ independent to the temperature and the sample. The exponential relaxation rate λ_{mag} , which parametrizes the muon spin relaxation caused by the (atomic) magnetism, are plotted in Fig. 3 as a function of temperature. The Néel temperature was defined as the temperature at which the exponential relaxation rate start to increase; the estimated Néel temperatures are shown in the figure.

III. DISCUSSION

The absence of muon spin precession in Pd doped samples indicates the fragility of the spatially homogeneous ordered moment sizes in Sr_2CuO_3 . With only less than one percent doping of Pd, the coherent precession of muon spin disappears, indicating that the ordered moment sizes have a broad spatial distribution under site dilution. The distribution of the moment sizes may be broader than in Zn- or Mg-doped CuGeO_3 , where muon spin precession was observed in the Néel state together with the exponential relaxation [21]. In the doped spin-Peierls compound, the distribution of the local field was consistent with the model that maximum moment size is induced near the doped center, and the moment size reduces exponentially with the coherence length ≈ 10 spin sites [21]. In $\text{Sr}_2(\text{Cu,Pd})\text{O}_3$ where the Cu moments are depleted by Pd impurities, the maximum moment should be located in the middle of the chain fragments as shown in Fig. 4. Because of the long coherence length expected for the gapless $S=1/2$ spin chain, the effect of the non-magnetic impurity may be extended in a large area; the maximum moment size of one chain-fragment might strongly depend on the chain length, and may not have a well-defined value in the doped system.

In Ref.[14], the μSR signal of the nominally undoped Sr_2CuO_3 was analyzed by assuming two muon sites each of which consists of one precession signal and one exponentially decaying signal. The latter was interpreted as $1/T_1$ relaxation of the local field component parallel to the initial muon spin orientation. The exponentially decaying terms describe the background relaxation which exhibits a fast front-end before $\approx 1\mu\text{s}$ as shown by the dashed line in Fig. 2a. The corresponding relaxation rate for the front-end ($\approx 5\mu\text{s}^{-1}$), however, is too large for the residual dynamics in the Néel ordered state. In this section, we calculate muon spin relaxation for the inhomogeneous Néel order with the existence of spin vacancies, from which the ordered moment size recovers exponentially with the recovery length ξ as shown in Fig. 4. The vacancies are the doped Pd ions or the impurities remaining in the nominally pure sample which manifest themselves as the Curie term in the magnetic susceptibility (Fig. 1). For the nominally pure Sr_2CuO_3 , the Curie term corresponds to the impurity level $\approx 0.04\%$ which corresponds to $L \approx 1/(2 \times 0.04 \times 10^{-2}) \approx 1000$ sites of

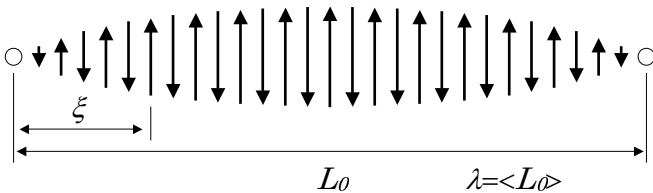


FIG. 4: Spatial evolution of the magnetic moment size assumed on a chain fragments. The small circles are the doped Pd sites, which were assumed to behave as an $S = 0$ impurity.

unperturbed spin-chain.

With the model shown in Fig. 4, the moment size $S(z)$ behaves as a function of the distance z from the end for a chain fragment with length L_0 :

$$S(z) = s_0 \left\{ 1 - \frac{\cosh((z - \frac{1}{2}L_0)/\xi)}{\cosh(\frac{1}{2}L_0/\xi)} \right\} \quad (3)$$

where s_0 is the moment size at infinity ($s_0 \approx 0.06\mu_B$) and ξ is the moment-size recovery length. By assuming that the muon local field H is proportional to the nearest moment size ($H(z) \propto S(z)$: local moment density approximation), the distribution function $\rho(H; L_0)$ of the local fields be obtained by the density of the states for the field H along the chain fragment L_0 :

$$\rho(H; L_0) = \frac{dz}{dH(z)}. \quad (4)$$

In the doped material, the impurity site should be located randomly. The experimentally observed field distribution function $\rho(H)$ in this situation is the average of $\rho(H; L_0)$ for the Poisson distribution of the chain length L_0 . The same procedure was taken for the model relaxation employed in the analysis of the μ SR spectra of doped CuGeO_3 [21].

The model muon relaxation function and the corresponding local field distribution function for the inhomogeneous ordered moment size (Fig. 4) are shown in Fig. 5. The behavior of the distribution function $\rho(H)$ is characterized by the ratio between the average chain-length $\lambda = \langle L_0 \rangle \approx 1/x$ and the moment-size recovery length ξ . In comparison to the model for doped CuGeO_3 (Fig. 4b of Ref. [21]), the local field distribution (Fig. 5b) has the same shape but the field axis is reversed between $H = 0$ and H_0 . This is because in the doped CuGeO_3 , impurities create magnetic moments, whereas in Sr_2CuO_3 moments are depleted from the chain. The role of the zero-field $H = 0$ and the maximum field $H = H_0$ are reversed between CuGeO_3 and Sr_2CuO_3 cases. As shown in Fig. 5a, when the ratio $\lambda/\xi \gg 1$, there is a coherent precession of muon spins because the moment size is relatively homogeneous and the local field distribution exhibits an isolated peak at $H = H_0$. As the ratio approaches unity, the precession amplitude is diminished and at $\lambda/\xi = 1$, only a weak bump remains at the position of the first precession peak. Below $\lambda/\xi = 0.5$, there

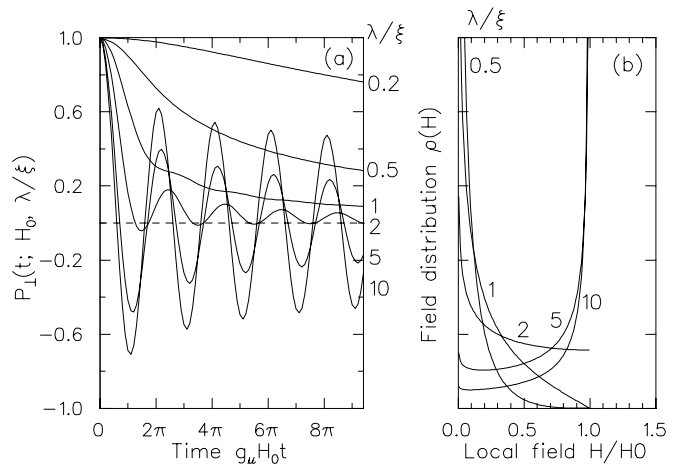


FIG. 5: (a) The muon relaxation function and (b) local-field distribution for the inhomogeneously Néel ordered spin-chain (Fig. 4).

is no visible oscillation and the relaxation is mostly exponential with time. Compared to the model for doped CuGeO_3 (Fig. 4b of Ref.[21]) with the same level of background relaxation, the amplitude of the precession signal component is much smaller in this model for depleted chains. The reason for the difference stems from the maximum moment size of the chain fragments: in the model of doped CuGeO_3 , it was assumed that the ends of all chains have the same induced moment size s_0 . In this model for depleted chains, the maximum moment size appears at the center of the chain fragments, and depends on their length.

If we represent the relaxation function shown in Fig. 5a with a symbol $P_{\perp}(t; H_0, \lambda/\xi)$, the muon relaxation function for one muon site becomes:

$$P_{\mu}(t) = A_{\perp}P_{\perp}(t; H_0, \lambda/\xi) + A_{\parallel}\exp(t/T_1), \quad (5)$$

where A_{\perp} (A_{\parallel}) is the amplitude of the local field component which is perpendicular (parallel) to the initial muon spin polarization, and T_1 is the spin-lattice relaxation time for the parallel component. As can be seen from the existence of two precession frequencies (Fig. 2a), there are two muon sites in Sr_2CuO_3 which, most likely, correspond to the muons attached to the in-chain and out-of-chain oxygen sites (see Appendix A). We introduced the local fields H_0^A and H_0^B for the each site, and obtained the following phenomenological function for the muon spin relaxation:

$$P_{\mu}(t) = A_{\perp}^A P_{\perp}(t; H_0^A, \lambda/\xi) + A_{\perp}^B P_{\perp}(t; H_0^B, \lambda/\xi) + A_{\parallel}^{A+B} \exp(t/T_1), \quad (6)$$

where A_{\perp}^A , A_{\perp}^B and A_{\parallel}^{A+B} are the amplitudes of each components. Here, the two $1/T_1$ signal components are combined in one relaxation amplitude (A_{\parallel}^{A+B}), since the background relaxation rate is too small to distinguish

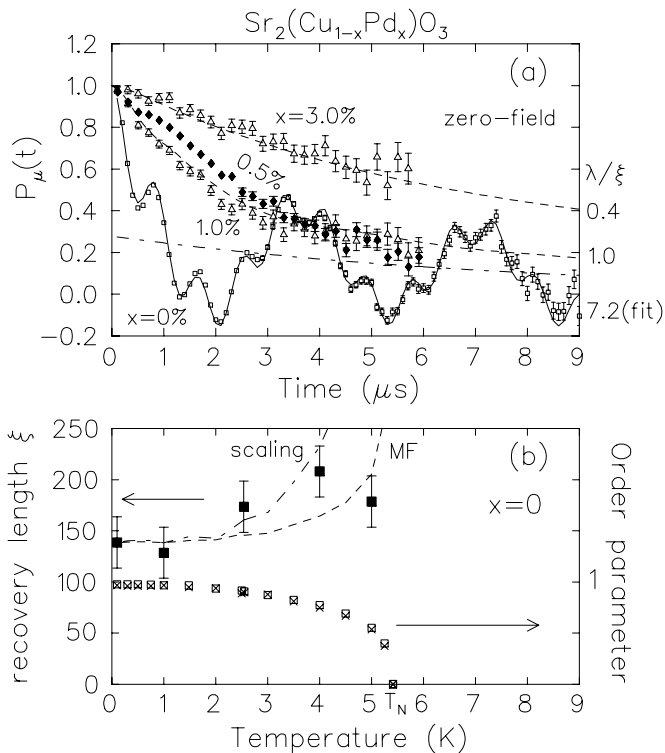


FIG. 6: (a) Muon spin relaxation in Sr_2CuO_3 analyzed with the relaxation function eq.(6) (solid line). The dot-dashed line is the contribution from the parallel-field term (A_{\parallel}^{A+B}) introduced in the analysis. Dashed lines are eq.(6) with the same parameters as in the $x = 0$ case, except the λ/ξ ratio. (b) Temperature dependence of the recovery length ξ and the magnetic order parameter as derived from the analysis. The dashed and the dot-dashed lines are the theoretical temperature dependence of ξ calculated from the experimental order parameter (see section III).

the contributions from the two sites. For the nominally pure sample, the precession signals can be analyzed with eq.(6). The solid line in Fig. 6a is the result of the fit and the dot-dashed line is the contribution from the $1/T_1$ relaxation term. It is noted that there are no extrinsic parameters introduced to describe the damping of the oscillation amplitude nor the early front-end relaxation. However, eq.(6) based on the inhomogeneous moment size distribution (Fig. 4) describes the over-all feature of the muon spin relaxation fairly well. The ratio between the average chain-length λ and the recovery length ξ yields $\lambda/\xi \approx 7.2$ from the analysis. The fast front-end relaxation at $t < 1\mu\text{s}$ is also described by the perpendicular terms (A_{\perp}^A and A_{\perp}^B). In this analysis, the $1/T_1$ relaxation rate is not as large as the one obtained in the previous analysis of Ref.[14].

The magnitude of the Curie term in the susceptibility for the nominally pure Sr_2CuO_3 (Table I) suggests the average chain-length for this nominally pure sample is $\lambda \approx 1/(2 \times 0.04\%) \approx 1000$ lattices. This and the ratio $\lambda/\xi = 7.2$ obtained from the fitting analysis suggests that

the recovery length of the moment size is $\xi \approx 150$ lattices, which is at least one order of magnitude longer than in the Néel state of doped CuGeO_3 in which $\xi \approx 10$ [21]. The absence of a nominal spin-gap in the $S = 1/2$ antiferromagnetic chain is most likely the cause for the correlation length being longer than in the doped spin-Peierls compound CuGeO_3 . The temperature dependence of the recovery length (ξ) and the magnetic order parameter ($\langle s_z \rangle \propto$ precession frequency) are plotted in Fig. 6b. The temperature dependence of ξ is weak and possibly exhibiting a slight increase at higher temperatures.

Based on the magnitude of the Curie terms, one can estimate the ratio λ/ξ for the Pd-doped compounds, which are summarized in Table I in parenthesis. The model relaxation functions eq.(6) for $\lambda/\xi = 1$ and 0.4 are shown as the dashed lines in Fig. 6a. These two parameter values corresponds to the Pd 0.5% and 3% doped samples, respectively. Since the μSR spectra of the doped systems do not exhibit the spectral features which were present in the $x = 0$ sample, it is not possible to experimentally determine the parameters in eq.(6). Here we assumed the same amplitudes (A_{\perp}^A , A_{\perp}^B and A_{\parallel}^{A+B}), local fields (H_0^A and H_0^B) and $1/T_1$ relaxation rate as determined in the $x = 0$ sample, and varied the λ/ξ parameter. This may be a good approximation in low doping in which the orientation of the local fields are approximately the same as in the nominally pure case. The calculated relaxation functions eq.(6) agree well with the behavior of the experimentally obtained μSR spectra of $\text{Sr}_2(\text{Cu}_{1-x}\text{Pd}_x)\text{O}_3$ as shown in Fig. 6a. Eventhough the μSR spectra in the Pd-doped samples do not show precession, this might originate in the static Néel order with spatial distribution of moment-sizes. The decoupling measurement (Fig. 2b) confirms that the relaxation is static, which is a support to the idea that it originates from Néel order. Because of the long recovery length ξ , the small amount of impurity ions disturbs the ordered-moment size in a large area, so that the spin precession of the local magnetic probe becomes invisible.

In the μSR time spectrum of the $x = 0.5\%$ sample, there is a hump in the measured polarization at $\approx 1\mu\text{sec}$ (Fig. 6a), at the position of the first precession peak for the nominally pure compound. From this result, it is suggested that the maximum moment size s_0 does not change in the sample with 0.5% Pd doping. For the $x = 1.0\%$ and 3.0% samples, such hump disappears, indicating that as the doping level increases, the parameter enters to the $\lambda/\xi \lesssim 1$ regime. The estimate of the λ/ξ value (Table I) confirms this conclusion.

In Fig. 7, the Néel temperature of $\text{Sr}_2(\text{Cu,Pd})\text{O}_3$ and the theoretical curve [13] are plotted. We estimate the average chain length L of $\text{Sr}_2(\text{Cu,Pd})\text{O}_3$ from the Curie term of the susceptibility, assuming that one Pd ion creates either $S = 0$ or $S = 1/2$ with the equal probability. The horizontal and vertical axes of Fig. 7 are normalized by the inter-chain interaction J' which has not been experimentally obtained for Sr_2CuO_3 . However the ratio $T_N/J = 4 \times 10^{-4}$ has been estimated [14] and the the-

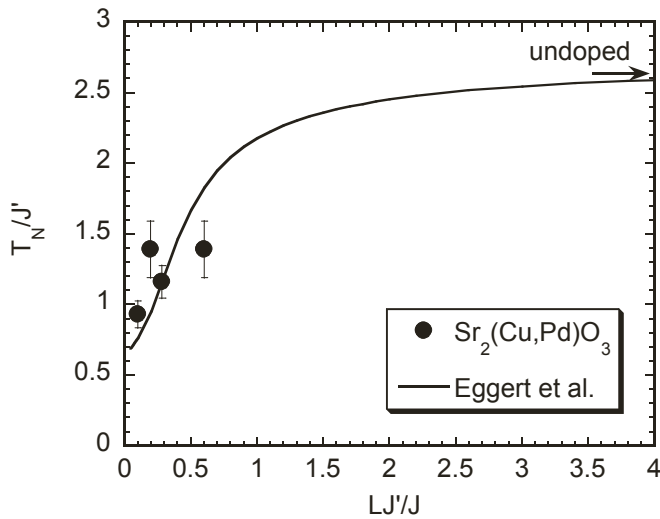


FIG. 7: Néel temperature vs. average chain length. The theoretical line is taken from Eggert *et al.* [13].

ory proposes $T_N/J' \approx 2.6$ in the long chain-length limit (Fig. 7). From these, one can obtain the ratio between the inter- and intra-chain couplings $J'/J \approx 1.6 \times 10^{-4}$. This value was employed to scale the average chain length L in the horizontal axis of Fig. 7. The agreement between theory and measurement regarding the Néel temperature is reasonably good, suggesting that the theory correctly estimates the energy scale of the magnetic order.

Within the same theoretical framework, the spatial distribution of the ordered moment size has been calculated recently [22]. The assumption made is that the $S = 1/2$ antiferromagnetic chain acquires the staggered moment size $\langle s_z \rangle$ in a consistent way from the effective staggered magnetic field B originating from the neighboring ordered chains. The intra-chain interaction J propagates the effect of the chain-end, reducing the ordered moment size at its vicinity. The inter-chain interaction J' recovers the ordered moment size by inducing the staggered magnetic field from the neighbouring chains. The competition between these two interactions on the chain fragments causes the spatial distribution of ordered moment sizes as shown in Fig. 4. A scaling argument proposes that the recovery length ξ is given by $\xi \propto B^{-2/3}$ [22, 23], where B is the effective staggered field. In the mean-field approximation, the staggered field can be written as $B = zJ'\langle s_z \rangle$, where J' is the inter-chain interaction, z is the number of neighboring chains and $\langle s_z \rangle$ is the magnetic order parameter. Combining these two relations, the recovery length in the mean-field approximation is given by $\xi_{MF} \propto \langle s_z \rangle^{-2/3}$. There is also a scaling relation between the magnetic order parameter and the staggered field: $\langle s_z \rangle \propto B^{1/3}$ [22]. With this and the scaling relation between ξ and B , one can obtain a scaling prediction for the recovery length: $\xi_{SC} \propto \langle s_z \rangle^{-2}$. In either case, the temperature dependence of the recovery length is set by that of the order parameter $\langle s_z \rangle$ but with

a different exponent.

The temperature dependence of the recovery length in the mean-field approximation (ξ_{MF}) and the scaling result (ξ_{SC}) are shown in Fig. 6b, based on the experimentally obtained magnetic order parameter. Since we do not know the over-all scale factor of the recovery length, we employed the experimental value obtained at low temperature. The experimental result is more consistent with the full scaling result ξ_{SC} , rather than with the value expected in the mean-field framework, except at the vicinity of the Néel temperature. The critical exponent of the order parameter as a function of temperature ($\beta \approx 0.2$) [21] also indicates that the system is in the scaling regime rather than in the three-dimensional mean-field regime in which $\beta \approx 0.5$. Our measurements suggest that the finite recovery length of the ordered moment sizes is determined by the effective staggered magnetic field B originating from the neighboring chains. The over-all scale factor $\xi/a \approx 150$ in the low temperature limit is yet to be calculated theoretically for the parameters of Sr_2CuO_3 .

In the theoretical calculation of chain fragments with the lengths longer than the recovery length ($L_0/\xi \gtrsim 1$), the self-consistent moment size exhibits a two peak structure in the distribution function (Fig. 1 of Ref.[22]). One peak is located almost at zero-moment size and the other appears at a slightly larger size than that for the unperturbed chain. The former and the latter peaks originate from the chain fragments with even and odd number of spins, respectively [22]. We have found that the Fourier transformation of the moment size distribution function exhibits clear precession, as a result of the isolated peak for the odd-numbered fragments. This theoretical result is in contrast to the experimental observation (Fig. 2a), in which the precession is damped upon doping. There are two possible explanations: (1) The moment size of the odd length chains may be reduced due to quantum fluctuations, as has already been suggested in Ref. [22]. (2) The sum of dipolar fields at the muon site contains contributions from neighboring chains, smearing out the even-odd effect. The proposed muon sites and the dipolar field calculations (Appendix A) demonstrate that the contribution from the nearest neighbor chain is actually dominant, at least for the higher frequency site. This suggests that the quantum fluctuation scenario (1) may be a more favoured explanation for the absence of muon spin precession in $\text{Sr}_2(\text{Cu,Pd})\text{O}_3$.

IV. CONCLUSIONS

We have investigated how Néel order is destructed with non-magnetic impurity doping in the quasi one-dimensional $S = 1/2$ antiferromagnet. The model material employed is $\text{Sr}_2(\text{Cu}_{1-x}\text{Pd}_x)\text{O}_3$. The susceptibility at $T > T_N$ exhibits Curie-Weiss behavior. The magnitude of the Curie term is consistent with a model in which the creation of half an induced moment (size = $1\mu_B$) occurs due to substitution with one Pd ion. This

suggests that the induced paramagnetic moment originates from the total spin of the chain fragments which is either $S = 0$ or $S = 1/2$ depending on the fragment consists of even or odd number of spin sites. The muon spin relaxation of the nominally pure Sr_2CuO_3 was re-analyzed with a model for the spatially inhomogeneous Néel ordered state. The length scale ξ was introduced to describe the recovery of ordered moment size away from the spin defect. It was suggested that the length scale ξ originates from the effective staggered magnetic field of the neighboring chains. The length scale $\xi \approx 150$ lattices for Sr_2CuO_3 is more than 10 times longer than in doped CuGeO_3 , which reflects the nominally gapless characteristic of the system.

In the Pd doped samples, the absence of muon spin precession for less than 1% doping level is consistent with a large recovery length ξ . The Néel temperature, which was defined as the temperature where muon spin relaxation rate starts to increase, exhibits a good agreement with recent theoretical calculation.

Acknowledgement

The authors would like to thank Dr. S. Eggert and Prof. I. Affleck for stimulating discussions. We also thank Prof. Y. Kato for valuable comments. The research in this paper has been financially supported by NEDO International Joint Research Grant and by COE & Grant-in-aid for Scientific Research from Monbusho. Work at Columbia University was supported by NSF-DMR-01-02752 and NSF-CHE-01-17752 (Nano-scale Science and Engineering Initiative).

APPENDIX A: MUON SITES

The crystal structure of Sr_2CuO_3 has two non-equivalent oxygen sites [15]. Site O(1) is out of the chain oxygen site of the corner-shared CuO_3 plaquette, and site O(2) is the shared oxygen of the two neighboring plaquettes forming the chain structure. In cuprates, it has been proposed that muons form an $\text{O}-\mu^+$ bond with oxygen ions in an analogy with the hydrogen bonding [24]. In this appendix, we calculate the electro-static potential for a muon which was assumed to form an $\text{O}-\mu$ bond with a bond length of 1\AA and determine the orientation of the bond with respect to the crystallographic axis. We also calculate the dipolar fields and compare with the experimentally observed local fields.

In Fig. 8a and 8b, contour plots of the electro-static potential are drawn for the muons forming the $\text{O}-\mu$ bonds with the O(1) site and O(2) site, respectively. The electro-static potential is calculated using the method of Ewald sum [25] assuming the formal point charges located at the ionic positions. The minimum of the potential exists at $(\theta, \varphi)_{(1)} = (60^\circ, 90^\circ)$ and $(\theta, \varphi)_{(2)} = (20^\circ, 0^\circ)$ for the O(1)- μ and O(2)- μ bonds, respectively,

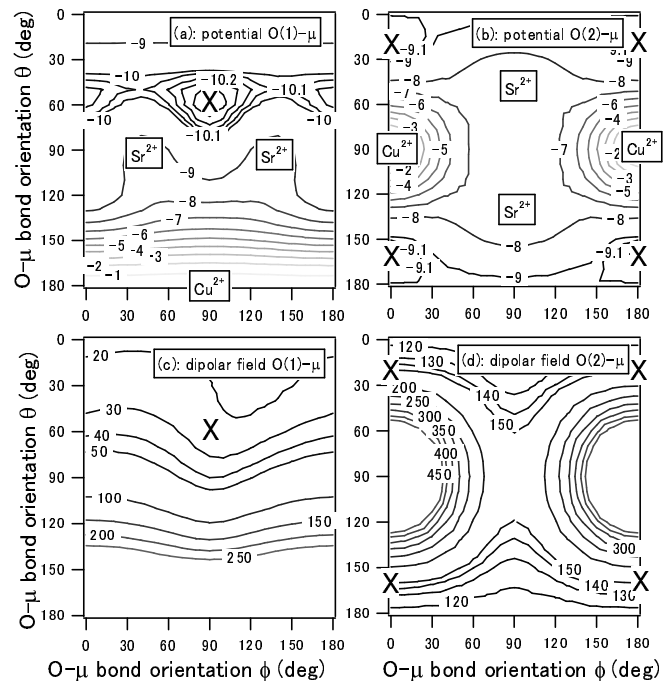


FIG. 8: (a) and (b): Electro-static potential for a muon 1\AA away from the oxygen site O(1) and O(2), respectively. The unit of the potential is in eV. The crosses are the potential minima which are the most probable orientation for the $\text{O}-\mu$ bond. (c) and (d): Dipolar fields calculated for the same $\text{O}-\mu$ bonding. The unit of the field is in Gauss for the spin structure determined by the neutron diffraction measurement [14].

which are shown by the cross symbol in the figures. The polar coordinate is defined as the $\theta = 0$ direction being parallel to the longest crystallographic axis (c -axis), and the $\varphi = 0^\circ$ direction in the basal plane being parallel to the CuO chains (a -axis). In Fig. 9, the muon sites in the real space crystal structure are shown by the star-symbols. The potential minimum value for the bond length of 1\AA is deeper for the O(1)- μ site (-10.4eV), than for the O(2)- μ site (-9.2eV). This suggests that O(2)- μ site may have a shorter bond-length to gain the electro-static potential of the oxygen ion.

The ordered moment size and its orientation of Sr_2CuO_3 has been obtained by neutron diffraction measurements as $0.06\mu_B$ pointing along the CuO chain direction, respectively [14]. The corresponding dipolar fields for the spin structure obtained are calculated for the two kinds of $\text{O}-\mu$ bonds. The results are shown in Fig. 8c and 8d. At the orientation of the minimum potential (cross symbols in the figures), the dipolar fields are 24G and 150G for the O(1)- μ and O(2)- μ site, respectively. The experimentally observed local fields in Sr_2CuO_3 are 23.3G and 97.7G [14]. The former is close to the calculation of O(1)- μ site, which is most likely the muon position responsible to the 23.3G signal. The 97.7G signal does not agree well with the calculation for the O(2)- μ site. The discrepancy might originate from the bond length which

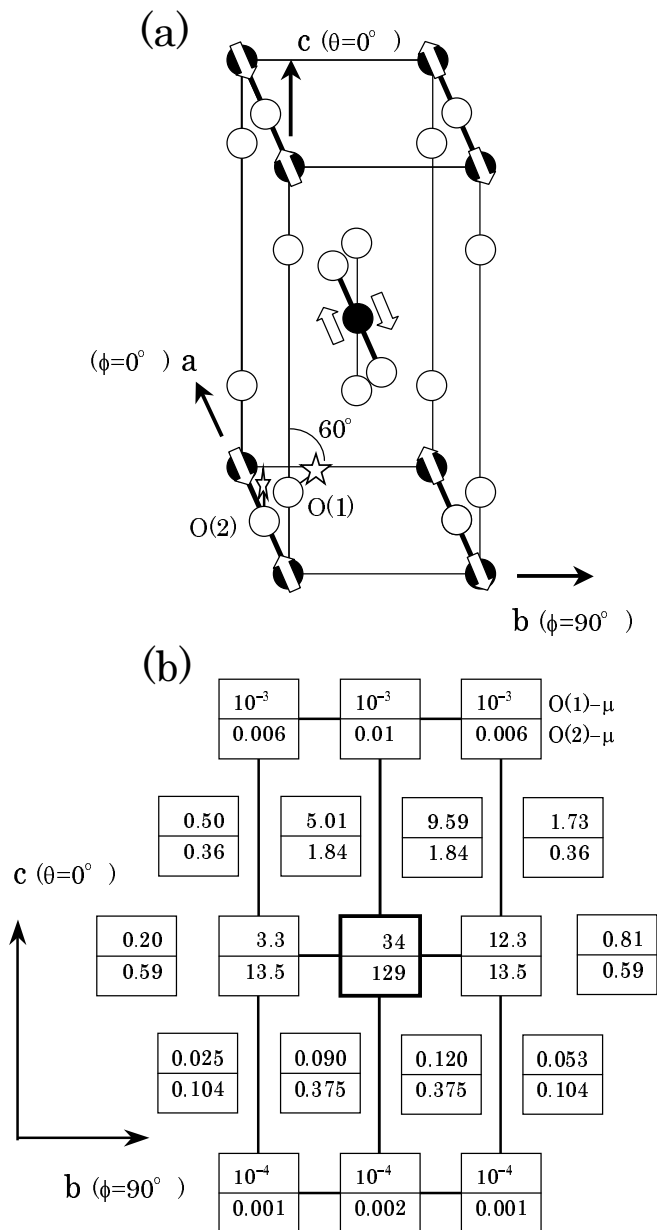


FIG. 9: (a) The crystal structure of Sr_2CuO_3 . O(1)- μ and O(2)- μ sites as determined by the electro-static potential calculation are shown by the star symbols which are attached to the oxygen sites. (b) The dipolar fields from the each chains to the muon sites. The boxes are distributed at the position of the chains seen along the a -axis. The upper and lower panels of the boxes are the dipolar fields for O(1)- μ and O(2)- μ sites, respectively. The unit of the fields is in Gauss.

could be shorter for O(2)- μ site. We have calculated the electro-static potential and the dipolar fields for a shortened O(2)- μ bond length of 0.9Å and found that the dipolar field at the potential minimum is reduced to 120G for the same spin structure. Since the pseudo minimum position for the O(1)- μ site $(60^\circ, 0^\circ)_{(1)}$ exhibits a much smaller dipolar field (40G), the 97.7G signal most likely originates from the O(2)- μ site with a shortened bond length.

For the muon sites proposed above, we calculate the contribution of the dipolar fields from neighboring chains. In Fig. 9b, we show the magnitude of the dipolar fields from the chains at the position of the boxes which represent the CuO chains projected to the $b \times c$ -plane. The upper and lower panels of the boxes indicates the dipolar fields of the O(1)- μ and O(2)- μ sites, respectively. For the O(1)- μ site, the contribution from the nearest neighboring chain is as large as 1/3 of the main contribution. This contribution from the neighboring chains broadens the local field distribution from that expected by the spatial distribution of the ordered moment sizes. However, the precession signal with higher frequency of the nominally pure Sr_2CuO_3 originates from the O(2)- μ site, at which the contribution of the dipolar field from the neighboring chains is at most 1/10 of the main contribution. This calculation suggests that the precession signal with higher frequency would survive, if the ordered moment size distribution has a distinctive peak at a finite frequency as proposed in the theoretical calculation [22]. The absence of the precession signal in the Pd-doped sample suggests that the isolated peak of the ordered moment size, which originates from the chain fragments with odd number of spins, is actually diminished in Sr_2CuO_3 due to the effects which are not included in the theoretical calculation.

- [1] B. Keimer, R.J. Birgeneau, A. Cassanho, Y. Endoh, R.W. Erwin, M.A. Kastner and G. Shirane, *Phys. Rev. Lett.* **67**, 1930, (1991).
 [2] B. Keimer, N. Belk, R.J. Birgeneau, A. Cassanho, C.Y. Chen, M. Greven, M.A. Kastner, A. Aharony, Y. Endoh, R.W. Erwin and G. Shirane, *Phys. Rev. B*

- 46**, 14034, (1992).
 [3] O.P. Vajk, P.K. Mang, M. Greven, P.M. Gehring and J.W. Lynn, *Science* **295**, 1691 (2002).
 [4] M. Hase, I. Terasaki, Y. Sasago, K. Uchinokura and H. Obara, *Phys. Rev. Lett.* **71**, 4059 (1993).
 [5] T. Masuda, A. Fujioka, Y. Uchiyama, I. Tsukada,

- K. Uchinokura, *Phys. Rev. Lett.* **80**, 4566 (1998).
- [6] M. Azuma, Y. Fujishiro, M. Takano, M. Nohara and H. Takagi, *Phys. Rev. B* **55**, R8658 (1997).
- [7] H. Fukuyama, T. Tanimoto and M. Saito *J. Phys. Soc. Jpn.* **65**, 1182 (1996).
- [8] H. Fukuyama, N. Nagaosa, T. Tanimoto and M. Saito *J. Phys. Soc. Jpn.* **65**, 2377 (1996).
- [9] D.C. Dender, P.R. Hammar, D.H. Reich, C. Broholm and G. Aeppli, *Phys. Rev. Lett.* **79**, 1750 (1997).
- [10] T. Asano, H. Nojiri, Y. Inagaki, J.P. Boucher, T. Sakon, Y. Ajiro, and M. Motokawa, *Phys. Rev. Lett.* **84**, 5880 (2000).
- [11] I. Affleck and M. Oshikawa, *Phys. Rev. B* **60**, 1038 (1999).
- [12] H. Schulz, *Phys. Rev. Lett.* **77**, 2790 (1997).
- [13] S. Eggert, I. Affleck and M.D.P. Horton, *Phys. Rev. Lett.* **89**, 047202 (2002).
- [14] K.M. Kojima, Y. Fudamoto, M. Larkin, G.M. Luke, J. Merrin, B. Nachumi, Y.J. Uemura, N. Motoyama, H. Eisaki, S. Uchida, K. Yamada, Y. Endoh, S. Hosoya, B.J. Sternlieb, and G. Shirane, *Phys. Rev. Lett.* **78**, 1787 (1997).
- [15] T. Ami, M.K. Crawford, R.L. Harlow, Z.R. Wang, D.C. Johnston, Q. Huang and R.W. Erwin, *Phys. Rev. B* **51**, 5994 (1995).
- [16] S. Eggert, *Phys. Rev. B* **53**, 5116 (1996).
- [17] N. Motoyama, H. Eisaki and S. Uchida, *Phys. Rev. Lett.* **76**, 3212 (1996).
- [18] Von H.-D. Wasel-Nielen and R. Hoppe, *Z. Anorg. Allg. Chem.* **375**, 209 (1970); Y. Nagata, T. Taniguchi, G. Tanaka, M. Satho and H. Samata, *J. Alloys and Compounds* **346**, 50 (2002).
- [19] R.S. Hayano, Y.J. Uemura, J. Imazato, N. Nishida, T. Yamazaki, R. Kubo, *Phys. Rev. B* **20**, 850 (1979).
- [20] Y.J. Uemura, T. Yamazaki, D.R. Harshman, M. Semba and E.J. Ansaldo, *Phys. Rev. B* **31**, 546 (1985).
- [21] K.M. Kojima, Y. Fudamoto, M. Larkin, G.M. Luke, J. Merrin, B. Nachumi, Y.J. Uemura, M. Hase, Y. Sasago, K. Uchinokura, Y. Ajiro, A. Revcolevschi, and J.-P. Renard, *Phys. Rev. Lett.* **79**, 503 (1997).
- [22] S.Eggert and I. Affleck, to appear in *J. Mag. Mag. Matr.* (2004).
- [23] S.Eggert, private communication (2004).
- [24] B. Hitti, P. Birrer, K. Fischer, F.N. Gygax, E. Lippelt, H. Maletta, A. Schenck, M. Weber, *Hyperfine Int.* **63**, 287 (1990).
- [25] C. Kittel, "Introduction to Solid State Physics" Appendix.